Proceedings of the ASME 2010 3rd Joint US-European Fluids Engineering Summer Meeting and 8th International Conference on Nanochannels, Microchannels, and Minichannels
FEDSM-ICNMM2010
August 1-5, 2010, Montreal, Canada

FEDSM-ICNMM2010-30913

EXPERIMENTAL STUDY OF SELF-EXCITED VIBRATION IN A THIN FILM WRAPPED AROUND AN AIR-TURN BAR

Kensuke Hara
Department of Mechanical Engineering
Aoyama Gakuin University
5-10-1 Fuchinobe, Chuo-ku, Sagamihara-shi,
Kanagawa, 252-5258, Japan
Email: hara@me.aoyama.ac.jp

Masahiro Watanabe
Department of Mechanical Engineering
Aoyama Gakuin University
5-10-1 Fuchinobe, Chuo-ku, Sagamihara-shi,
Kanagawa, 252-5258, Japan
Email: watanabe@me.aoyama.ac.jp

ABSTRACT

This paper describes an experimental study for a self-excited vibration in the thin film wrapped around an air-turn bar. The characteristics of a self-excited vibration are investigated by obtaining time histories of the film deflection and distributions of a steady pressure and a pressure fluctuation at a surface of the air-turn bar. The experimental results show that this system has two different types of vibration modes. One is a low-frequency mode which the film vibrates radially with respect to the the air-turn bar. The other is a high-frequency mode which the film flaps in the out-of-plane direction of the film. Moreover, a stability diagram of the self-excited vibration is obtained by changing the flow rate and the tensile force acting on the film. It is shown that the low-frequency vibration mode occurs when the flow rate and the tensile force are large, and the high-frequency vibration mode occurs at any flow rate and tensile force in this experiment.

INTRODUCTION

An air turn-bar is a hollow, cylindrical drum with slits which is set to inject air. It is used in web handling applications where it is important to change the transport direction of a thin film without contacts. The thin film is supported by an air cushion in a clearance between the thin film and the air turn-bar formed by injecting air through the slit. The thin film floats the air cushion and the transport direction of the thin film can be changed without contacts between the thin film and the air turn-bar. However, it is reported that self-excited vibrations occur in the wrapped thin film caused by a fluid structure interaction between the thin film and the injecting air.

Up to this time, some applications of using the air cushion to transport techniques without contact have been proposed [1–7]. Chang and Moretti reported aerodynamic characteristics of pressure pad air bars [1]. Deflections of webs in air-flotation ovens are analyzed by Moretti [2]. Hashimoto studied the air film thickness and friction characteristics on stationary guides in web handling processes [3, 4]. Müftü et al. proposed analytical method to calculate the fluid mechanics of the air cushion [5]. Moreover, the steady pressure distributions and the web deflection of the air-turn bar were analyzed [6, 7]. Other application of using the air cushion is a flow dynamic conveyor. Ishihara reported that the self-excited vibration occurs in the flow dynamic conveyor [8,9]. On the other hand, there are many works for the self-excited vibration of a flexible sheet and a web due to air flow [10–14]. However, it is not clarified that vibration characteristics and instability condition of the self-excited vibration generated in the film wrapped around the air-turn bar.

In this study, we conducted the experiment to investigate the characteristics of the self-excited vibration in the thin film wrapped around the air-turn bar. Time histories of film displacement and distributions of pressure in the clearance between the film and the air turn-bar are obtained by the experiment. Moreover, instability conditions are investigated by changing the flow rate and the tensile force acting on the thin film. After that, the

characteristics of self-excited vibration are discussed.

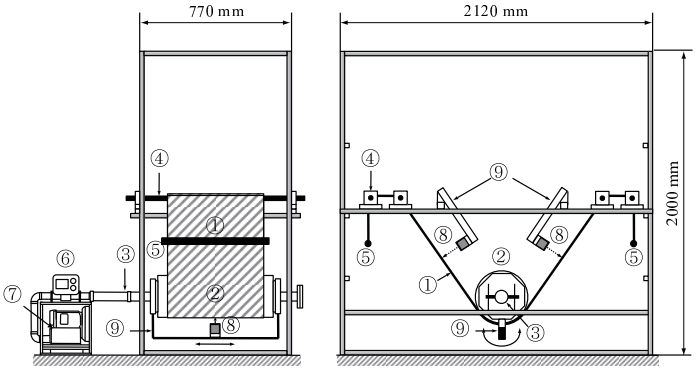

FIGURE 1. Schematic view of experimental setup

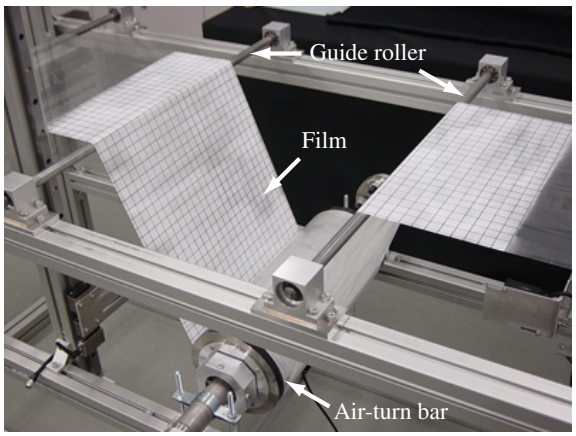

FIGURE 2. Photograph of experimental setup

EXPERIMENT

Experimental Setup

Figures 1 and 2 show the schematic view and the photograph of the experimental setup, respectively. The major parameters used in the experiment are given in Table 1. The pressurized air injected into the air-turn bar is generated by a blower. The air cushion is formed in the clearance between the thin film and the air-turn bar by injecting pressurized air through the slits of air-turn bar. The thin film floats over this air cushion. A PET film having a width of 450 [mm] and a thickness of 16 [μm] is used as the thin film, which is supported by guide rollers and the air cushion formed by the air-turn bar. The tensile force is applied to the thin film using weights which are hung at both ends of the thin film.

Air-turn Bar

Figure 3 shows a schematic depiction of the air-turn bar used in this experiment. The details of the air-turn bar is given in Table 2. The air-turn bar has three slits to inject pressurized air every 45-degree. These slits have the width of 3 mm and the length of 450 mm. The air-turn bar is set that the middle slit of air-turn bar is directed downward in a vertical direction.

TABLE 1. Major parameters used in the experiment

Film material		PET
Width of film	[mm]	450
Thickness of film	[μm]	16
Wrapped angle	[deg]	90
Mass of weights	[kg]	1.0 - 5.0
Flow rate	[$\times 10^{-3}\mathrm{m}^3/\mathrm{s}$]	2.5 - 20.8

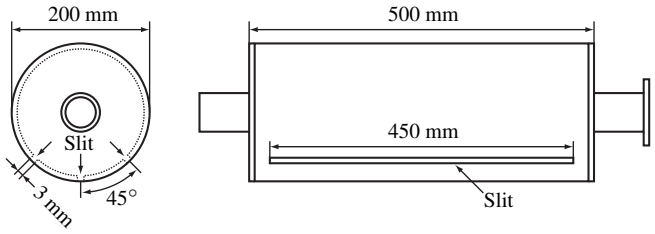

FIGURE 3. Schematic view of air-turn bar

TABLE 2. Dimensions of the air-turn bar used in the experiment

Diameter [mm]	Length [mm]	Slit width [mm]	Slit length [mm]
200	500	3	450

TABLE 3. Details of data collection and processing

		Film deflection	Pressure
Sensor type		Laser	Differential pressure
Sample rate	[Hz]	500	500
Sample number		4096	4096

Measurement System

A schematic view of a measurement system for the film deflection is shown in Figure 4. The nonwrapped region is the flat

region of the thin film between the guide roller and the edge of air-turn bar. On the other hand, the wrapped region is the curved region of the thin film from the left to right edges of air-turn bar. The wrapped angle θ is equal to the wrapped region when the thin film contacts the air-turn bar. In this experiment, the wrapped angle is set at $\theta = 90$ [deg]. The vibration displacement is measured by three laser sensors. Two sensors are set at Points A and B, which are the center of the nonwrapped regions. On the other hand, a sensor is set at Point C, which is the center of the wrapped region. Figure 5 shows a schematic view of a pressure measurement system. Distributions of a steady pressure and a pressure fluctuation in the clearance between the air-turn bar and the thin film are measured by pressure sensors set at the surface of the air-turn bar. In this paper, the pressure distributions are shown by using $\xi-$coordinate, which is defined as the coordinate system along the surface of the air-turn bar, as shown in Figure 5.

The signals of these sensors are amplified by the amplifier. Then, the data logger records the amplified signals. The details of the methods used for data collection and processing are written in Table 3.

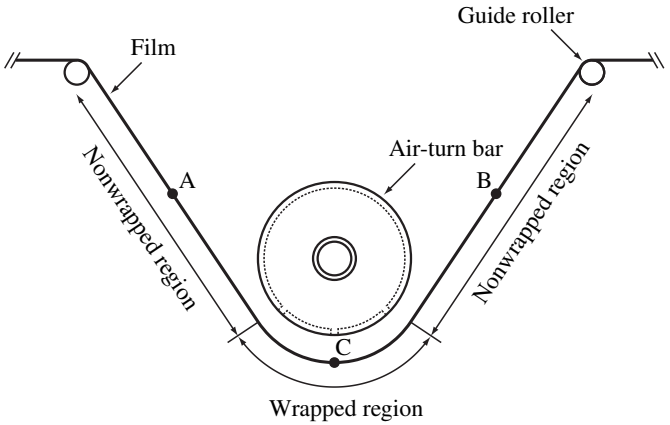

FIGURE 4. Schematic view of film deflection measurement system

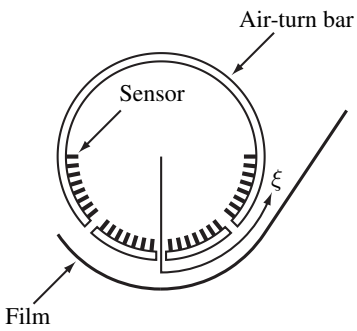

FIGURE 5. Schematic view of pressure measurement system

RESULTS

Film Deflection and Dominant Frequency

Figures 6, 7 and 8 show the typical results of the root mean square (RMS) values of vibration displacement and the dominant frequencies of thin film at Points A, B and C, respectively. In Figure 6(a), the horizontal axis indicates the flow rate Q. On the other hand, the vertical axis represents the RMS values of vibration displacement of thin film at Point A. This figure shows that the RMS values of vibration displacement increase rapidly at $Q = 5.83$ [$\times 10^{-3}$ m^3/s]. Then, the RMS values increase gradually between $Q = 5.83$ [$\times 10^{-3}$ m^3/s] and $Q = 9.17$ [$\times 10^{-3}$ m^3/s].

The dominant frequencies of the self-excited vibration are shown in Figure 6(b). In this figure, the horizontal and the vertical axes represent the flow rate Q and the dominant frequency, respectively. From Figure 6(b), it can be seen that the dominant frequencies of measured vibration in Figure 6(a) are about 50 Hz, which is an almost constant value between $Q = 5.83$ [$\times 10^{-3}$ m^3/s] and $Q = 9.17$ [$\times 10^{-3}$ m^3/s].

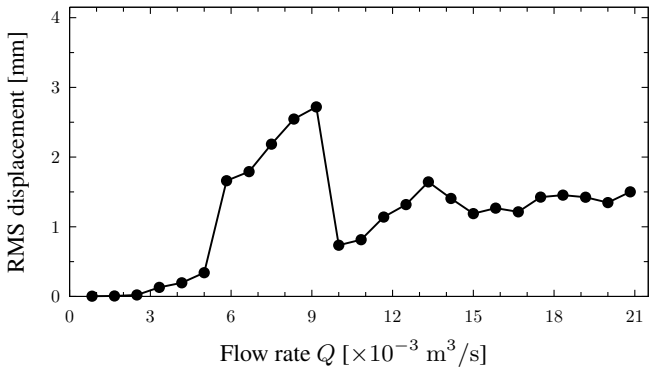

(a) RMS values of vibration displacement

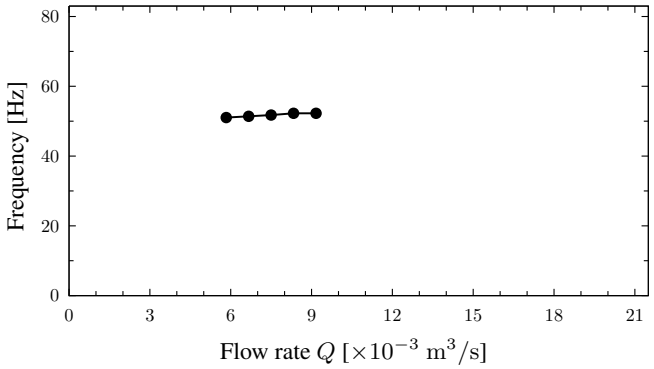

(b) Dominant frequency of vibration displacement

FIGURE 6. RMS displacement and dominant frequency of vibration of the thin film at Point A ($T = 124.3$ [N/m], $\theta = 90$ [deg])

The RMS values of vibration displacement and the dominant frequencies at Point B are shown in Figure 7. These results are similar to the results at Point A. Figure 7(a) shows that the large values of vibration displacement are measured between $Q = 5.00$ [$\times 10^{-3}$ m^3/s] and $Q = 9.17$ [$\times 10^{-3}$ m^3/s]. The dominant frequencies of these vibrations are shown in Figure 7(b). From this figure, it can be seen that the dominant frequencies of the vibrations at Point B correspond to those at Point A.

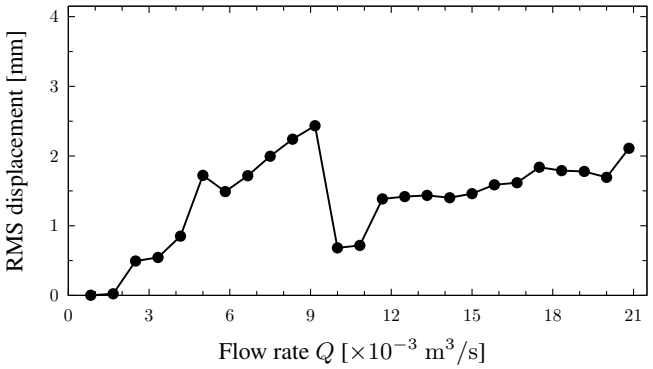

(a) RMS values of vibration displacement

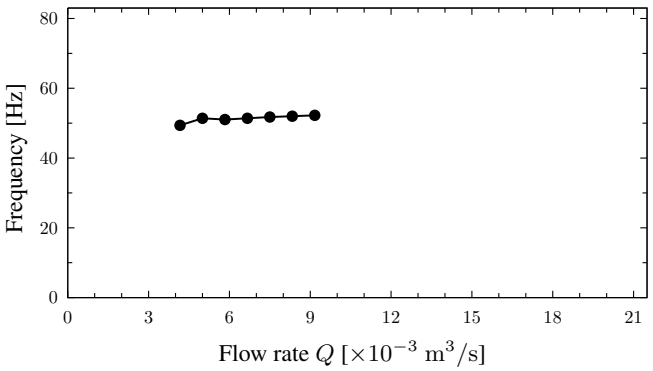

(b) Dominant frequency of vibration displacement

FIGURE 7. RMS displacement and dominant frequency of vibration of the thin film at Point A ($T = 124.3$ [N/m], $\theta = 90$ [deg])

Figure 8 shows the RMS values of vibration displacement and the dominant frequencies of thin film at Point C. These results differ from those at Point A and B. The RMS values of vibration displacement at Point C remain small in the flow rate range of $Q = 5.00$ [$\times 10^{-3}$ m^3/s] and $Q = 9.17$ [$\times 10^{-3}$ m^3/s], where the vibration displacements at Points A and B became large. In contrast, the vibration displacements increase when the flow rate Q is more than 11.7 [$\times 10^{-3}$ m^3/s].

The dominant frequencies of vibration displacement are shown in Figure 8(b). It can be seen that the dominant frequencies of measured vibration in Figure 8(a) are about 6.7 Hz. This dominant frequency is considerably lower than those at Points A and B.

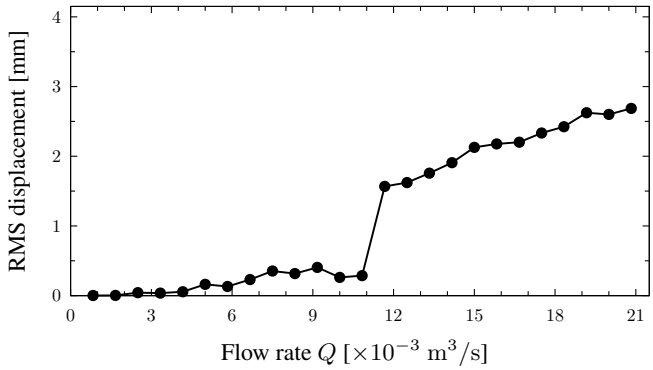

(a) RMS values of vibration displacement

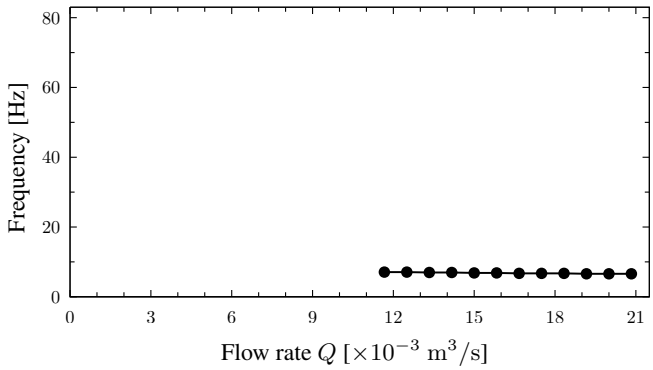

(b) Dominant frequency of vibration displacement

FIGURE 8. RMS displacement and dominant frequency of vibration of the thin film at Point A ($T = 124.3$ [N/m], $\theta = 90$ [deg])

Time Histories of the Thin Film

Figures 9, 10 and 11 show the time histories of vibration displacement of the thin film at Points A, B and C in the case of the low flow rate ($Q = 5.83 \times 10^{-3}$[m^3/s]), respectively. In these figures, the horizontal axis shows the time. On the other hand, the vertical axis represents the vibration displacement of thin film. From these Figures, the vibration displacements of the Points A and B are considerably larger than the results of Point C. Moreover, the dominant frequency of this vibration is 50.8 [Hz]. This results indicate that, in the low flow rate region, only the nonwrapped regions of the thin film flaps largely in the out-of-plane direction of the film with high frequency.

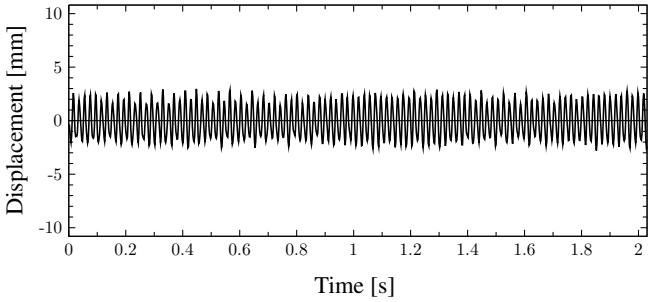

FIGURE 9. Time history of the displacement of the thin film at Point A ($T = 124.3$ [N/m], $\theta = 90$ [deg])

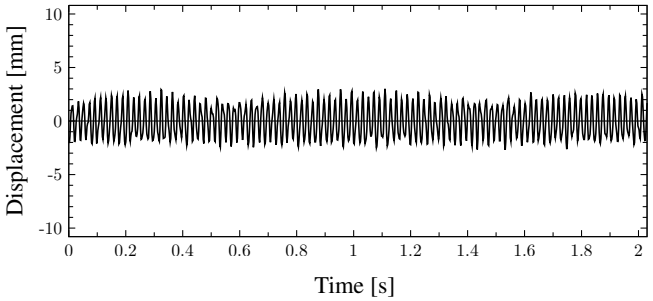

FIGURE 10. Time history of the displacement of the thin film at Point B ($T = 124.3$ [N/m], $\theta = 90$ [deg])

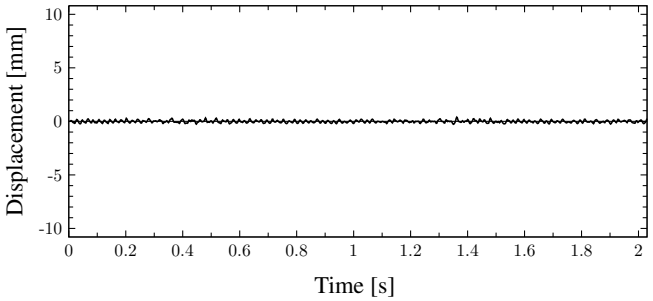

FIGURE 11. Time history of the displacement of the thin film at Point C ($T = 124.3$ [N/m], $\theta = 90$ [deg])

Figures 12, 13 and 14 show the time histories of vibration displacement of the thin film at Points A, B, and C in the case of the high flow rate ($Q = 20.8 \times 10^{-3}[\mathrm{m}^3/\mathrm{s}]$), respectively. In the high flow rate region, the vibration displacement of the Point C is larger than that in the case of the low flow rate. Moreover, the dominant frequency of this vibration is 6.7 [Hz]. In this situation, it is shown that the thin film slides largely along the air-turn bar with low frequency.

Based on these results, it is shown that there are two different types of self-excited vibration in this system, as shown in Figure 15. One is a low-frequency vibration mode which the film vibrates radially with respect to the the air-turn bar and the center of wrapped region vibrates largely in the vertical direction. This vibration mode occurs in the case of high flow rate. The other is a high-frequency vibration mode which only the nonwrapped regions of the thin film flap largely in the out-of-plane direction of the thin film. In contrast to the low-frequency vibration mode, the high frequency vibration mode occurs in the case of low flow rate.

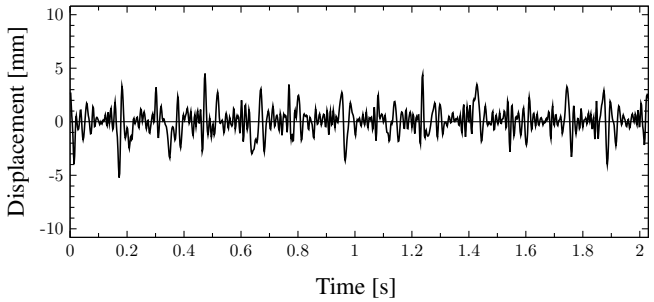

FIGURE 12. Time history of the displacement of the thin film at Point A ($T = 124.3$ [N/m], $\theta = 90$ [deg])

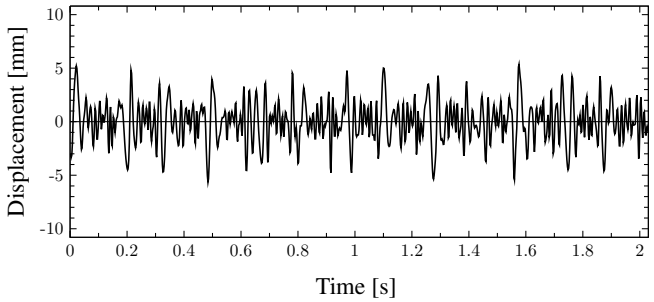

FIGURE 13. Time history of the displacement of the thin film at Point B ($T = 124.3$ [N/m], $\theta = 90$ [deg])

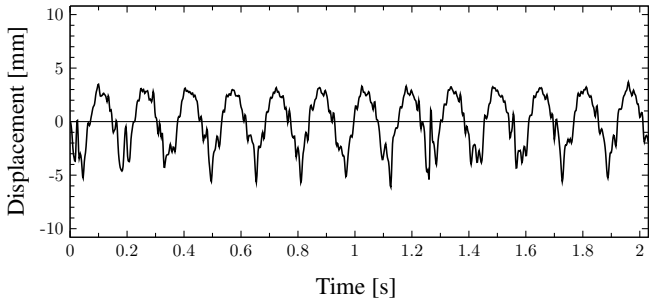

FIGURE 14. Time history of the displacement of the thin film at Point C ($T = 124.3$ [N/m], $\theta = 90$ [deg])

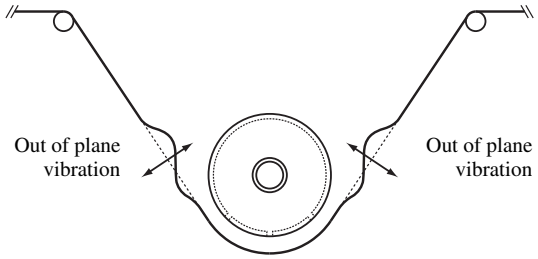

(a) High-frequency vibration mode

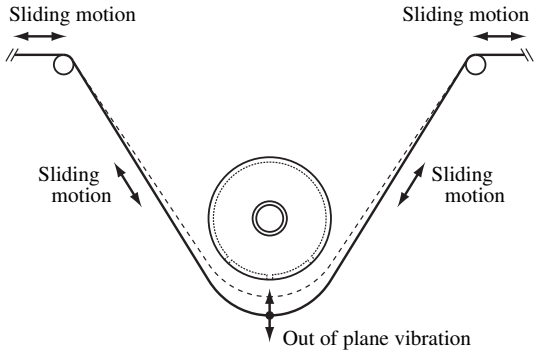

(b) Low-frequency vibration mode

FIGURE 15. Vibration mode of the wrapped thin film around the air-turn bar

Distribution of Steady Pressure

Figure 16 shows a steady pressure distribution in the wrapped region and the nonwrapped region when the flow rate is $Q = 5.83 \times 10^{-3}[\mathrm{m}^3/\mathrm{s}]$. In this figure, the horizontal axis shows measurement points at the surface of the air-turn bar. On the other hand, the vertical axis represents the steady pressure. From this figure, the steady pressure in the wrapped region is larger than that in the nonwapped region because of injection of the pressurized air. The steady pressure decreases rapidly at $\xi = 78.5$ [mm]. Moreover, the steady pressure is negative at $\xi = 78.5$ [mm], and it can be seen that a pressure spike at the boundary of the wrapped region and the nonwrapped region.

A steady pressure distribution in the case of $Q = 20.8 \times 10^{-3}[\mathrm{m}^3/\mathrm{s}]$ is shown in Figure 17. In this case, the steady pressure distribution is similar to the result in the case of $Q = 5.83 \times 10^{-3}[\mathrm{m}^3/\mathrm{s}]$. From this figure, the pressure rapidly drops at $\xi = 78.5$ [mm]. Moreover, the values of the steady pressure distributions are about the same as those in the case of $Q = 5.83 \times 10^{-3}[\mathrm{m}^3/\mathrm{s}]$.

By comparing Figure 16 and Figure 17, the steady pressure distributions remain nearly constant, even though more pressurized air is injected into the clearance between the air-turn bar and the thin film.

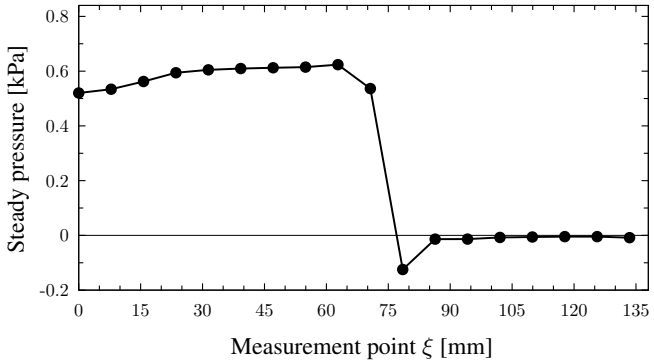

FIGURE 16. Steady pressure distribution of the high-frequency vibration mode at the surface of air-turn bar ($Q = 5.83 \times 10^{-3}$ [m^3/s])

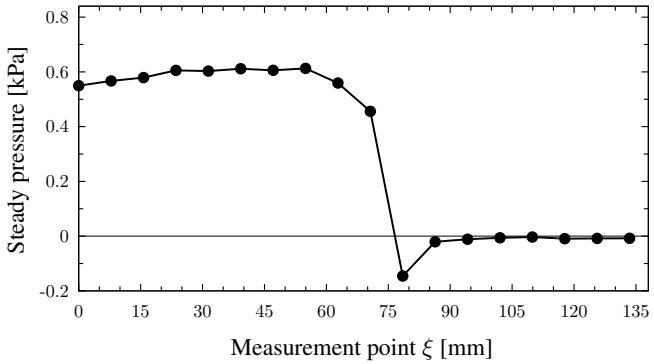

FIGURE 17. Steady pressure distribution of the low-frequency vibration mode at the surface of air-turn bar ($Q = 20.8 \times 10^{-3}$ [m^3/s])

Distribution of Pressure Fluctuation

Figures 18 and 19 show distributions of the pressure fluctuation in the wrapped region and the nonwrapped region when the flow rates Q are $5.83 \times 10^{-3}[\mathrm{m}^3/\mathrm{s}]$ and $20.8 \times 10^{-3}[\mathrm{m}^3/\mathrm{s}]$, respectively. In these figures, the horizontal axis shows the measurement points at the surface of the air-turn bar. On the other hand, the vertical axis represents the RMS values of the pressure fluctuation. In figures 18 and 19, the dashed lines show the steady pressure distributions shown in Figs. 16 and 17, respectively. From figure 18, the pressure fluctuation is small in the case of $Q = 5.83 \times 10^{-3}[\mathrm{m}^3/\mathrm{s}]$. In particular, the pressure fluctuation in the wrapped area is almost equal to zero. However, the pressure fluctuation increases locally at the edge of the air-turn bar ($\xi = 78.5$[mm]). On the other hand, Figure 19 shows that the pressure fluctuation in the wrapped region is considerably larger than that in the nonwrapped region, in the case of $Q = 20.8 \times 10^{-3}[\mathrm{m}^3/\mathrm{s}]$, when the low-frequency vibration mode occurs. From figures 18 and 19, it can be seen that the pressure fluctuation in the case of $Q = 20.8 \times 10^{-3}[\mathrm{m}^3/\mathrm{s}]$ is considerably larger than that in the case of $Q = 5.83 \times 10^{-3}[\mathrm{m}^3/\mathrm{s}]$

in the wrapped region. In contrast to the results of the wrapped region, it can be seen that the pressure fluctuations in the non-wrapped region are small.

Based on these results, it is shown that the low-frequency vibration mode is generated by the large pressure fluctuation in the wrapped region. On the other hand, the generation of high-frequency vibration mode is related to the local pressure increase near the edges of air turn-bar.

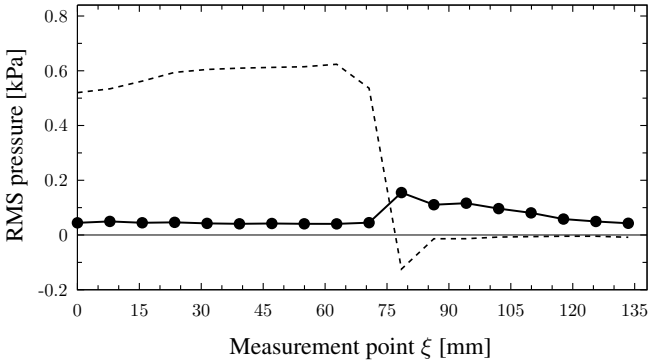

FIGURE 18. Distribution of pressure fluctuation of the high-frequency vibration mode at the surface of air-turn bar ($Q = 5.83 \times 10^{-3}$ [m^3/s])

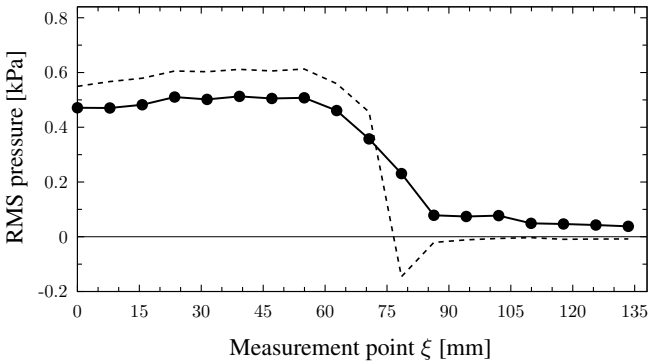

FIGURE 19. Distribution of pressure fluctuation of the low-frequency vibration mode at the surface of air-turn bar ($Q = 20.8 \times 10^{-3}$ [m^3/s])

Stability Diagram

In order to obtain the instability regions of the low-frequency and high-frequency vibration modes, the experiment was conducted with changing the flow rate of the pressurized air Q and the tensile force T. In this experiment, the flow rate Q was varied between 2.50×10^{-3} [m^3/s] and 20.8×10^{-3} [m^3/s], and the tensile force T was varied between 28.4 [$\mathrm{N/m}$] and 124.3 [$\mathrm{N/m}$]. The experimental results of the stability diagram are shown in Figure 20. The horizontal axis shows the tensile force T. Moreover, the vertical axis represents the flow rate Q. In this figure, ○ shows the instability region of the high-frequency vibration mode, and ● shows the instability region of low-frequency vibration mode. It can be seen that the region of the high-frequency vibration mode is distributed over the entire region in Figure 20. In contrast to the high-frequency mode, the low-frequency mode occurs when the tensile force and the flow rate are large.

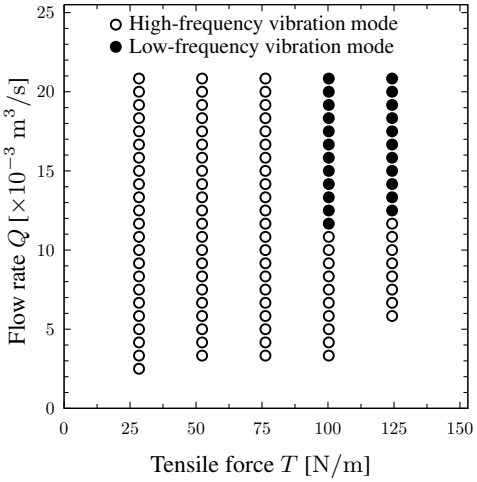

FIGURE 20. Stability diagram

CONCLUSIONS

In this study, we investigated the characteristics of the self-excited vibration in the thin film wrapped around the air-turn bar by the experiment. As a result, it was shown that this system has two different types of the self-excited vibration. The characteristics of these vibration modes are as follows.

One is the low-frequency vibration mode which the film vibrates radially with respect to the the air-turn bar. This vibration mode occurred when the tensile force and the flow rate are large. Moreover, the pressure fluctuations in the wrapped region became large when the low-frequency vibration was observed.

The other is the high-frequency vibration mode which the film flaps in the out-of-plane direction of the thin film. In contrast to the low-frequency vibration mode, this vibration mode occurred without the effects of changing the tensile force and the flow rate. Moreover, the distribution of the pressure fluctuations indicates that the generations of the high-frequency vibrationnal mode are related to the local pressure increase near the edges of air turn-bar.

ACKNOWLEDGMENT

This work was supported by Japan Society for the Promotion of Science (JSPS), Grant-in-Aid Scientific Research (C) 20560225. The authors are grateful to graduate students, Kazuki Uehara and Yasuharu Igarashi, for the experimental assistance.

REFERENCES

[1] Chang, Y. B., and Moretti, P. M., Aerodynamics Characteristics of Pressure-Pad Air Bars, *Transactions of the ASME*, *Journal of Applied Mechanics*, Vol.67 (2000), pp.177-182.

[2] Moretti, P. M., Lateral Deflections of Webs in Air-Flotation Ovens, *Transactions of the ASME*, *Journal of*, Vol.71 (2004), pp.314-320.

[3] Hashimoto, H., and Nakagawa, H., Air Film Thickness Estimation in Web Handling Processes , *Transactions of the ASME*, *Journal of Tribology*, Vol.121 (1999), pp.50-55.

[4] Hashimoto, H., and Nakagawa, H., Improvement of Web Spacing and Friction Characteristics by Two Types of Stationary Guides, *Transactions of the ASME*, *Journal of Tribology*, Vol.123 (2001), pp.509-516.

[5] Müftü , S., Lewis, T. S., Cole, K. A., and Benson, R. C., A Two-Dimensional Model of the Fluid Dynamics of an Air Reverser, *Transactions of the ASME*, *Journal of Applied Mechanics*, Vol.65 (1998), pp.171-177.

[6] Müftü , S., and Cole, K. A., The Fluid-Structure Interaction in Supporting a Thin Flexible Cylindrical Web with an Air Cushion, *Journal of Fluid and Structures*, Vol.13 (1999), pp.681-708.

[7] Müftü , S., Mechanics of a Thin, Tensioned Shell, Wrapped Helically around a Turn-Bar, *Journal of Fluids and Structures*, Vol.23 (2007), pp.767-785.

[8] Ishihara, K., On Abnormal Vibration Generated in Flow Dynamic Conveyor, *Proceedings of PVP2007*, (2007), Paper No.PVP2007-26131, Texas, USA.

[9] Ishihara, K., Study on Generation Mechanism of Abnormal Vibration of Flow Dynamic Conveyer, *Proceedings of PVP2009*, (2009), Paper No.PVP2009-77212, Prague, Czech Republic.

[10] Watanabe, Y., Suzuki, S., Sugihara, M, and Sueoka, Y., An Experimental Study of Paper Flutter, *Journal of Fluids and Structures*, Vol.16, (2002), pp.529-542.

[11] Watanabe, Y., Isogai, K., Suzuki, S., and Sugihara, M., A Theoretical Study of Paper Flutter, *Journal of Fluids and Structures*, Vol.16, (2002), pp.543-560.

[12] Guo, C. Q., and Paidoussis, M. P., Stability of Rectangular Plates with Free Side-Edges in Two-Dimensional Inviscid Channel Flow, *Transactions of the ASME*, *Journal of Applied Mechanics*, Vol.67, (2000), pp.171-176.

[13] Tang, L., and Paidoussis, M. P., On the Instability and the Post-Critical Behavior of Two-Dimensional Cantilevered Flexible Plates in Axial Flow, *Journal of Sound and Vibration*, Vol.305, (2007), pp.97-115.

[14] Wu, X., and Kaneko, S., Linear and Nonlinear Analysis of Sheet Flutter Induced by Leakage Flow, *Journal of Fluids and Structures*, Vol.20, (2005), pp.927-948.